



**HAL**  
open science

## The trisulfur radical ion $S_3^{\bullet-}$ controls platinum transport by hydrothermal fluids

Gleb S Pokrovski, Maria A Kokh, Elsa Desmaele, Clément Laskar, Elena F Bazarkina, Anastassia y Borisova, Denis Testemale, Jean-Louis F Hazemann, Rodolphe Vuilleumier, Guillaume Ferlat, et al.

► **To cite this version:**

Gleb S Pokrovski, Maria A Kokh, Elsa Desmaele, Clément Laskar, Elena F Bazarkina, et al.. The trisulfur radical ion  $S_3^{\bullet-}$  controls platinum transport by hydrothermal fluids. Proceedings of the National Academy of Sciences of the United States of America, 2021, 118 (34), pp.e2109768118. 10.1073/pnas.2109768118 . hal-03323512

**HAL Id: hal-03323512**

**<https://hal.science/hal-03323512>**

Submitted on 23 Aug 2021

**HAL** is a multi-disciplinary open access archive for the deposit and dissemination of scientific research documents, whether they are published or not. The documents may come from teaching and research institutions in France or abroad, or from public or private research centers.

L'archive ouverte pluridisciplinaire **HAL**, est destinée au dépôt et à la diffusion de documents scientifiques de niveau recherche, publiés ou non, émanant des établissements d'enseignement et de recherche français ou étrangers, des laboratoires publics ou privés.



1  
2 **Main Manuscript for**

3  
4 **The trisulfur radical ion  $S_3^{\cdot-}$  controls platinum transport by hydrothermal fluids**

5  
6 **Gleb S. Pokrovski<sup>1,\*</sup>, Maria A. Kokh<sup>1,5</sup>, Elsa Desmaele<sup>2</sup>, Clément Laskar<sup>1</sup>, Elena F.**  
7 **Bazarkina<sup>3,6</sup>, Anastassia Y. Borisova<sup>1,7</sup>, Denis Testemale<sup>3</sup>, Jean-Louis Hazemann<sup>3</sup>,**  
8 **Rodolphe Vuilleumier<sup>2</sup>, Guillaume Ferlat<sup>4</sup>, and Antonino Marco Saitta<sup>4</sup>**

9 <sup>1</sup>Experimental Géosciences Team (GeoExp), Géosciences Environnement Toulouse (GET), UMR 5563 CNRS,  
10 Université Paul Sabatier Toulouse III, IRD, CNES, Observatoire Midi-Pyrénées, 14 av. Edouard Belin, F-31400  
11 Toulouse, France.

12 <sup>2</sup>PASTEUR, Département de Chimie, École Normale Supérieure, PSL University, Sorbonne Université, CNRS, F-75005  
13 Paris, France.

14 <sup>3</sup>Université Grenoble Alpes, CNRS, Institut Néel, 25 av. des Martyrs, F-38042 Grenoble Cedex 9, France.

15 <sup>4</sup>Sorbonne Université, CNRS, UMR 7590, IMPMC, F-75005 Paris, France.

16 <sup>5</sup>Universität Potsdam, Institut für Geowissenschaften, Campus Golm, Haus 27, Karl-Liebknecht-Str. 24-25, D-14476  
17 Potsdam, Germany.

18 <sup>6</sup>Institute of Geology of Ore Deposits, Petrography, Mineralogy and Geochemistry, Russian Academy of Sciences (IGEM  
19 RAS), 35, Staromonetny per., F-119017 Moscow, Russia.

20 <sup>7</sup>Geological Department, Lomonosov Moscow State University, Vorobievsky Gory, Moscow, Russia

21  
22 \*G.S. Pokrovski, phones: +33-5-61-33-26-18; +33-6-20-34-72-62; E-mail: gleb.pokrovski@get.omp.eu;  
23 glebounet@gmail.com

24  
25 **Author contributions:**

26 G.S.P. designed research and wrote the paper; M.A.K., E.D., D.T., C.L., R.V. and G.S.P. performed  
27 experiments and modeling; C.L., E.F.B., A.Y.B., J-L.H., G.F. and A.M.S. contributed new  
28 reagents/analytical/computational tools; G.S.P., M.A.K., E.D. analyzed data; all authors contributed to  
29 data interpretation and manuscript preparation.

30  
31 **Competing Interest Statement:** The authors declare no competing interests.

32 **Classifications:** Physical - Earth, Atmospheric and Planetary Science

33 **Keywords:** platinum, sulfur, hydrothermal fluid, platinum group elements, trisulfur ion

34 **This PDF file includes:**

35 Main Text (incl. abstract, significance statement, ms text, references and figure captions = 4700 words)

36 Figures 1 to 3 (uploaded separately)

37 References 1 to 33

41 **Abstract (177 words):**

42 Platinum group elements (PGE) are considered to be very poorly soluble in aqueous fluids in  
43 most natural hydrothermal-magmatic contexts and industrial processes. Here we combined in  
44 situ X-ray absorption spectroscopy and solubility experiments with atomistic and  
45 thermodynamic simulations to demonstrate that the trisulfur radical ion  $S_3^{\bullet-}$  forms very stable  
46 and soluble complexes both with  $Pt^{II}$  and  $Pt^{IV}$  in sulfur-bearing aqueous solution at elevated  
47 temperatures ( $\sim 300^\circ C$ ). These novel Pt-bearing species enable (re)mobilization, transfer, and  
48 focused precipitation of platinum up to 10,000 times more efficiently than any other common  
49 inorganic ligand such as hydroxide, chloride, sulfate or sulfide. Our results imply a far more  
50 important, than believed so far, contribution of sulfur-bearing hydrothermal fluids to PGE  
51 transfer and accumulation in the Earth's crust. This discovery challenges traditional models of  
52 PGE economic concentration from silicate and sulfide melts, and provides new possibilities for  
53 resource prospecting in hydrothermal shallow-crust settings. The exceptionally high capacity of  
54 the  $S_3^{\bullet-}$  ion to bind platinum may also offer new routes for PGE selective extraction from ore  
55 and hydrothermal synthesis of noble metal nanomaterials.

56

57

58 **Significance Statement (118 words):** Platinum group elements (PGE) are highly valued by  
59 many industrial applications, serve as important geochemical tracers of planetary processes, and  
60 are among eagerly sought natural resources of critical trace metals. We show here that aqueous  
61 sulfur-bearing fluids play a far more important role, than believed, in many natural and  
62 technological processes in which PGE are involved. This role is essentially ensured by the  
63 radical sulfur ion  $S_3^{\bullet-}$  that forms extremely stable and soluble complexes both with  $Pt^{II}$  and  $Pt^{IV}$ .  
64 By enabling enhanced dissolution, transport and precipitation of Pt, these species may be key  
65 players in PGE transfer, fractionation, and accumulation in the Earth's crust. They may also offer  
66 novel opportunities for optimizing ore processing and nanomaterial synthesis.

67

68

69 **Main Text**

70 **Introduction**

71           The increasing use of platinum in high-technology fields spanning from the automotive and  
72 petrochemical industries to pharmaceuticals and nanomaterials, combined with its scarcity in nature  
73 (average Pt content in upper continental crust rocks is ~0.5 ng/g), makes Pt a highly valued  
74 commodity and eagerly sought natural resource (1-3). Currently assessed georesources of  
75 platinum group elements (PGE) are rare and mostly occur in mafic magmatic settings where PGE  
76 are concentrated in Fe-Ni-Cu sulfide minerals and melts (2-5). Their formation models are built on  
77 purely magmatic differentiation including fractional crystallization and sulfide-silicate partitioning  
78 and currently lack a robust assessment of the role of aqueous fluids. Indeed, systematic findings of  
79 inclusions of fluids and hydrous minerals in giant PGE magmatic deposits such as Bushveld,  
80 Norilsk, Sudbury (6-8) and in PGE-enriched mantle-derived rocks and lavas (9, 10) point to the  
81 potential role of post-magmatic aqueous fluids in PGE transfer and redistribution. Furthermore,  
82 there is multiple evidence of remobilization and concentration of Pt, as well as other PGE, in  
83 various low-to-moderate temperature (200–500°C) hydrothermal environments such as porphyry  
84 Cu-Au-Mo and metamorphic and sedimentary-hosted Au deposits, black shales, and serpentinites  
85 (4, 11), with Pt concentrations 1000 times its average crustal abundance, making such settings  
86 potentially exploitable for PGE. Therefore, knowledge of Pt chemical speciation and solubility in  
87 the hydrothermal fluid phase is required to quantify the formation and distribution of Pt resources  
88 in nature, to use PGE as geochemical tracers of Earth formation and evolution (e.g., 9, 10), as well  
89 as to optimize the rapidly growing Pt use in technological processes involving both aqueous and  
90 organic solvents (e.g., 1, 12-14).

91 Paradoxically, existing data on aqueous complexes of divalent  $\text{Pt}^{\text{II}}$ , which is a typical  
92 oxidation state of platinum in nature, with most common inorganic ligands such as chloride ( $\text{Cl}^-$ ),  
93 sulfate ( $\text{SO}_4^{2-}$ ), and hydroxide ( $\text{OH}^-$ ) (15-17) yield far too small metal aqueous contents ( $<0.1$   
94  $\text{ng/g}$ ) in equilibrium with Pt-bearing mineral phases to account for the observed Pt mobility in most  
95 fluids below the magmatic-hydrothermal transition ( $<600\text{--}700^\circ\text{C}$ ). Such fluids, produced by  
96 magma degassing or metamorphism or circulating in sedimentary basins, are commonly near-  
97 neutral ( $4 < \text{pH} < 8$ ), moderately saline ( $<20 \text{ wt\% NaCl}$ ), and often sulfur-bearing (up to 1–3 wt% S)  
98 containing both sulfide and sulfate. Because of the high chemical affinity of Pt for reduced sulfur  
99 (18), hydrogen sulfide ( $\text{HS}^-$ ) complexes are more plausible agents to transport Pt by such fluids.  
100 However, the reported data on their thermodynamic stability and the resulting solubility of Pt  
101 sulfide solids are highly controversial, spanning over almost 4 orders of magnitude, from  $<0.1 \text{ ng/g}$   
102 Pt in reduced  $\text{H}_2\text{S}$ -dominated fluids (19-21) to  $>1000 \text{ ng/g}$  Pt in oxidized sulfide/sulfate-bearing  
103 fluids (22). Such discrepancies call upon complexes other than sulfide (and sulfate) and/or metal  
104 oxidation states other than  $\text{Pt}^{\text{II}}$  to account for platinum solubility.

105 The current speciation models of PGE in aqueous media ignore, in particular, the trisulfur  
106 radical ion,  $\text{S}_3^{\cdot-}$ , well-known in sulfur non-aqueous chemistry (23) and stable across a very wide  
107 temperature ( $T$ ) and pressure ( $P$ ) range of magmatic-to-epithermal sulfate/sulfide-bearing fluids  
108 (24-28). Moreover, this ligand was recently shown to bind to gold greatly enhancing the efficiency  
109 of Au supply to hydrothermal-magmatic porphyry and metamorphic ore deposits associated with  
110 subduction zone settings which commonly involve S-rich fluids (29). To quantify the effect of  $\text{S}_3^{\cdot-}$   
111 on Pt behavior in typical hydrothermal fluids, we used in situ X-ray absorption spectroscopy  
112 (XAS, including both near-edge structure or XANES, and extended fine structure or EXAFS) that  
113 provides a direct fingerprint of metal redox, coordination and ligand identity. The spectroscopic

114 data were combined with solubility measurements and quantum-chemistry and thermodynamic  
115 modeling of Pt speciation in aqueous sulfide/sulfate/S<sub>3</sub><sup>•-</sup> solutions saturated with platinum sulfide  
116 solid PtS(s) at 275–300°C and 500–700 bar (*SI Appendix*).

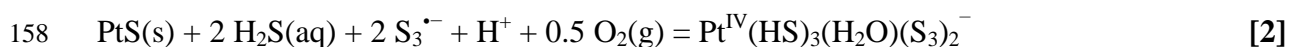
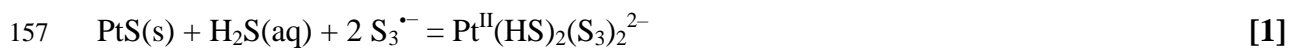
117

## 118 **Results**

119 Platinum L<sub>3</sub>-edge XANES spectra of S<sub>3</sub><sup>•-</sup> bearing solutions show a systematic evolution as  
120 a function of pH and redox (expressed in log<sub>10</sub> (bars) scale relative to the conventional hematite-  
121 magnetite *f*<sub>O<sub>2</sub></sub> mineral buffer, HM, *Fig. 1A*). Spectra of the near-neutral (pH 5.9 at 275°C) and  
122 relatively reduced (HM–0.2) solution are close to that of Pt<sup>II</sup>S(s) both in energy position and  
123 amplitude, fully consistent with divalent Pt<sup>II</sup> coordinated by 4 nearest S atoms in a square-planar  
124 geometry. By contrast, for more acidic and oxidized compositions, the spectra show a systematic  
125 shift to higher energies along with an increase in the white-line amplitude (*Fig. 1A*), indicating a  
126 change to higher Pt oxidation state and coordination, which would be closer to those of Pt<sup>IV</sup>S<sub>2</sub>(s) in  
127 which Pt is octahedrally coordinated by 6 S atoms. This trend is confirmed by quantum-chemistry  
128 simulations of XANES spectra (*SI Appendix*) by considering complexes with HS<sup>-</sup> and S<sub>3</sub><sup>•-</sup> ligands  
129 of square-planar and octahedral coordination geometry typical for Pt<sup>II</sup> and Pt<sup>IV</sup> compounds,  
130 respectively (18). The spectrum from the HM–0.2 solution closely resembles the simulation for  
131 square-planar Pt<sup>II</sup>(HS)<sub>2</sub>(S<sub>3</sub>)<sub>2</sub><sup>2-</sup>, whereas the spectrum from the HM+0.8 solution is best matched by  
132 octahedral Pt<sup>IV</sup>(HS)<sub>3</sub>(H<sub>2</sub>O)(S<sub>3</sub>)<sub>2</sub><sup>-</sup> (*Fig. 1B*). In contrast, none of the experimental spectra resembles  
133 the simulation for Pt<sup>II</sup>(HS)<sub>4</sub><sup>2-</sup> (*Fig. 1B*) or other analogous [Pt<sup>II</sup>(HS)<sub>*n*</sub>(H<sub>2</sub>O)<sub>4-*n*</sub><sup>2-*n*</sup>]-type species  
134 commonly adopted in the literature (19-21), thus strongly supporting the predominance of new  
135 [S<sub>3</sub><sup>•-</sup>]-type species at our conditions.

136           These findings are fully supported by the EXAFS data that show a systematic increase of  
 137 the first-shell mean Pt-S distance (from 2.32 to  $2.36 \pm 0.007$  Å, 2 SD), and coordination number  
 138 (from 4 to  $5 \pm 0.5$  S atoms, 2 SD), from the most reduced and least acidic (HM-0.2, pH 5.9) to the  
 139 most oxidized and most acidic (HM+0.8, pH 4.9) solutions, along with the presence of  $2 \pm 1$  second-  
 140 shell S atoms at  $3.50 \pm 0.02$  Å in the second Pt shell of all solutions (*SI Appendix*, Figs. S2-S4;  
 141 Table S1). Oxygen neighbors that may stem from OH groups or H<sub>2</sub>O molecules in the Pt nearest  
 142 atomic shell, were found to be below the detection limit of  $\leq 1$  O atom (*SI Appendix*). The  
 143 amplitude of changes of the 1<sup>st</sup> shell Pt-S distances ( $>0.04$  Å) and coordination numbers (from 4 to  
 144 5) with  $f_{O_2}$  and pH (*SI Appendix*, Fig. S4) definitely implies a mixture of different species, and  
 145 cannot be explained by the presence of only divalent Pt<sup>II</sup>-S complexes, which are commonly square  
 146 planar and have a very narrow range of Pt-S<sub>4</sub> distances (2.30–2.32 Å; e.g., refs. 18, 30). Therefore,  
 147 our findings are more consistent with the presence of both Pt<sup>II</sup> and Pt<sup>IV</sup> species in variable  
 148 proportions in solution. Furthermore, the detection of 2<sup>nd</sup> shell S atoms provides compelling  
 149 evidence for the presence of the S<sub>3</sub><sup>•-</sup> ligand in both types of Pt complexes.

150           Using these key constraints from in situ spectroscopy, we applied thermodynamic modeling  
 151 to the two sets of PtS(s) solubility data, one obtained simultaneously with the XAS spectra at  
 152 275°C/700 bar (Figs. S1A, S5, Table S1) and the other from batch-reactor measurements at  
 153 300°C/500 bar conducted within similar ranges of redox, pH and solution composition (Figs. S1B,  
 154 2, Table S2). Both datasets were found to be consistent with the formation of two complexes,  
 155 Pt<sup>II</sup>(HS)<sub>2</sub>(S<sub>3</sub>)<sub>2</sub><sup>2-</sup> and Pt<sup>IV</sup>(HS)<sub>3</sub>(H<sub>2</sub>O)(S<sub>3</sub>)<sub>2</sub><sup>-</sup>, that control the solubility at near-neutral pH/more  
 156 reducing conditions and acidic pH/more oxidizing conditions, respectively (Fig. 2):



159 Fig. 2 shows that the presence of relatively minor concentrations of  $S_3^{\bullet-}$  in solution (~10 mmol,  
 160 versus >100 mmol of  $H_2S/HS^-$ ) leads to 4 to 5 order-of-magnitude enhancement of PtS(s)  
 161 solubility compared to predictions for the commonly assumed hydrogen sulfide complexes from  
 162 literature data obtained using reduced  $H_2S$ -dominated solutions (19, 21). The relative affinities of  
 163  $Pt^{II}$  to the  $S_3^{\bullet-}$  and  $HS^-$  ligands may be evaluated using a symmetrical ligand exchange reaction  
 164 between  $Pt^{II}(HS)_2(S_3)_2^{2-}$  and the  $Pt(HS)_4^{2-}$  complex of the same electric charge and coordination:



166 The value of the reaction [3] equilibrium constant at 300°C and 500 bar is  $10^{8.7}$  as derived by  
 167 combining the data of this study (Tables S3 and S5) and those for  $Pt(HS)_4^{2-}$  from ref. (19). This  
 168 value means that the affinity of  $Pt^{II}$  for one  $S_3^{\bullet-}$  ligand is at least  $\sim 10^4$  greater than for one  $HS^-$   
 169 ligand. Such remarkable affinity to  $S_3^{\bullet-}$  may be related to a favorable combination of the electronic  
 170 configurations of both  $Pt^{II}$  having two empty 5d shell orbitals ( $[Xe]4f^{14}5d^86s^0$ ) and the radical  $S_3^{\bullet-}$   
 171 ion having an unpaired electron to fill these orbitals in a chemical bond, coupled with favorable  
 172 steric factors yielding a highly stable symmetrical complex geometry with 2  $S_3^{\bullet-}$  ligands in trans-  
 173 position (Fig. 1B). Remarkably, the affinities of aurous gold ( $Au^I$ ) for  $S_3^{\bullet-}$  and  $HS^-$  are very similar  
 174 as attested by an equilibrium constant of  $\sim 1$  for an analogous ligand exchange reaction:  $Au(HS)_2^- +$   
 175  $S_3^{\bullet-} = Au(HS)(S_3)^- + HS^-$ , studied across a temperature range of 200–500°C (29). Compared to  $Pt^{II}$   
 176 or  $Pt^{IV}$ ,  $Au^I$  has its 5d shell filled ( $5d^{10}$ ), which may render bonding with the different sulfur  
 177 ligands less specific. Furthermore, the 4 and 6-coordinated geometries of Pt offer more flexibility  
 178 and less steric strain for binding to 2  $S_3^{\bullet-}$  ligands, compared to  $Au^I$  whose stable coordination is  
 179 limited to quasi-linear geometries (L-Au-L, e.g., refs. 29, 33). These tendencies are also in good  
 180 agreement with the generally more chalcophile (i.e. sulfur loving) character of Pt that forms far  
 181 more stable (poly)sulfide solid phases than those formed by Au (e.g., 18, 30). The equilibrium



182 constant values derived for reactions [1] and [2] (Table S5) allow Pt solubility predictions across  
183 the wide compositional range of natural and technological S-bearing hydrothermal fluids (Fig. 3).

184

## 185 **Discussion and Applications**

186 The discovery of stable soluble platinum-trisulfur ion complexes in aqueous fluids offers  
187 new applications in geoscience, chemistry and material science.

188 First, the large enhancement of Pt solubility in hydrothermal ore-forming fluids in the  
189 presence of  $S_3^{\bullet-}$  explains the multiple cases of PGE enrichment in a variety of hydrothermal sulfide  
190 deposits of common metals (Cu, Mo, Zn, Au, Ag), which may become a novel economic source of  
191 platinum in near future. Our predictions of Pt solubility (Fig. 3) show that  $\mu\text{g/g}$  levels of metal  
192 concentrations may easily be transported by typical epithermal fluids at temperatures around  
193  $300^\circ\text{C}$ . Our predictions are in marked contrast with former models based on 'traditional' sulfide  
194 and chloride ligands that account for less than  $\text{ng/g}$  levels of Pt in such fluids. Consequently,  
195 breakdown of  $S_3^{\bullet-}$  within rather narrow S concentration (0.1–1 wt%), pH (3–7) and  $f_{O_2}$  (HM $\pm$ 1)  
196 windows upon the evolution of a S-rich hydrothermal fluid would yield focused Pt precipitation in  
197 high tenors from a fluid volume  $10^3$  to  $10^5$  times smaller than would be required to precipitate the  
198 same platinum amount if the [Pt- $S_3$ ] complexes were ignored. Compared to gold, whose speciation  
199 is dominated by hydrogen sulfide complexes in most hydrothermal solutions of near-neutral pH  
200 below  $350^\circ\text{C}$  ( $\text{Au}(\text{HS})_2^-$ ; Fig. 3D) because of the much greater abundance of the  $\text{HS}^-/\text{H}_2\text{S}$  ligands  
201 than  $S_3^{\bullet-}$ , platinum mobility is far more strongly enhanced in the presence of even small amounts  
202 of  $S_3^{\bullet-}$ . Therefore, this ligand may control the fractionation of PGE from Au as well as other more  
203 common metals such as Cu, Zn, Pb, or Ni. These metals have a weaker chemical affinity to  $S_3^{\bullet-}$

204 and their speciation is dominated by complexes with far more abundant chloride in most  
205 hydrothermal fluids (29).

206         Second, on a larger mantle-crust scale, S-bearing aqueous fluids may play a far more  
207 important role in PGE behavior than believed. Even though our exploratory data set does not  
208 currently allow extrapolations to higher, closer to magmatic, temperatures, the growing stability  
209 of  $S_3^{\bullet-}$  as well as of its higher-temperature (>500°C) counterpart  $S_2^{\bullet-}$  (26, 28), suggests that both  
210 radical ions may play a key role in PGE mobility in hydrothermal-magmatic systems. As a  
211 result, the radical ions may promote PGE transfers from deep magmas or metamorphic rocks in  
212 subduction zones to aqueous fluids and their massive transport up to shallow crust settings,  
213 thereby explaining the observed PGE enrichment in gold and base metal porphyry-epithermal  
214 deposits, black-shale sedimentary environments, and serpentinites. Our findings of stable PGE  
215 complexes with  $S_3^{\bullet-}$ , if further confirmed across a wider *T-P* range, may shift the long-standing  
216 paradigms on PGE deposit formation by purely magmatic processes, in the light of multiple  
217 evidence of aqueous fluid presence (6-8, 11). Quantifying the role of such S-bearing fluids  
218 requires more systematic data on PGE interactions with the sulfur radical ions over the  
219 magmatic-hydrothermal *T-P* range. Our results demonstrating a strong Pt enrichment in S-  
220 bearing fluids, in which the aqueous sulfate and sulfide forms of sulfur coexist, may offer novel  
221 perspectives in the exploration of alternative PGE economic sources in hydrothermal settings  
222 that host both sulfate and sulfide mineral assemblages. Furthermore, our study points to an  
223 important role of slab-derived fluids under redox conditions of the sulfate-sulfide coexistence  
224 common in subduction zones and favoring the abundance of  $S_3^{\bullet-}$  and  $S_2^{\bullet-}$  (e.g., 28). Such fluids,  
225 often enriched in sulfur, may be capable of selectively mobilizing Pt and, by analogy,  
226 electronically similar  $Pd^{II}$  and  $Ir^I$ , from the mantle wedge. On the other hand, other, less

227 chalcophile PGE such as Ru, Rh or Os, generally having weaker affinities for soft ligands like  
228 (poly)sulfides (18), would be much less affected. These differences in the affinity to  $S_3^{\bullet-}$  may  
229 thus induce fluid-mineral fractionations among different PGE thereby impacting their both  
230 elemental and isotopic signatures in mantle-derived rocks that are widely used as geochemical  
231 tracers of planetary accretion and core-mantle evolution (e.g., 9, 10).

232 Third, the discovery of highly soluble  $S_3^{\bullet-}$  complexes with both  $Pt^{II}$  and  $Pt^{IV}$  may open  
233 new routes for hydrothermal synthesis of PGE-based nanomaterials increasingly used in  
234 catalysis, medicine, and electronics. Trisulfur ion may offer an interesting alternative to organic  
235 thiolate ligands currently used as precursors in the synthesis of Au and Pt nanoparticles and  
236 their stabilization in solution (31, 32). Furthermore, the specific solubility pattern of PtS(s) and,  
237 by analogy, of Pt metal as a function of solution pH and redox potential, passing through a  
238 maximum at slightly acidic pH and an  $H_2S/SO_4$  ratio of ~4, corresponding to the maximum of  
239  $S_3^{\bullet-}$  abundance (Fig. 3), may be explored for optimizing Pt nanoparticle preparation and  
240 functionalization both through reduction/oxidation and acidification/basification. Such unique  
241 solubility dependence thus offers greater flexibility and a larger redox, pH and temperature  
242 window for synthesis protocols both in aqueous or organic solvents than those currently based  
243 on  $H_2$  reduction of  $Pt^{II}$  chloride or thiolate complexes unstable at elevated temperatures (e.g.,  
244 12-14). Our findings thus extend the choice of S-ligands and provide more potential for tuning  
245 the molecular mechanisms that control the shape, atomicity, structure, and resulting reactivity of  
246 the formed nanoparticles of noble metals.

247

248 **Methods Summary** (See *SI Appendix* for detailed description of experimental and model  
249 systems, methods, and uncertainties)

250

251 **X-Ray Absorption Spectroscopy and Solubility Measurements.** Platinum solubility and chemical  
252 molecular speciation were investigated in aqueous PtS(s)-saturated solutions of thiosulfate and elemental  
253 sulfur that yield variable equilibrium amounts of hydrogen sulfide ( $\text{H}_2\text{S}/\text{HS}^-$ ), (hydrogen)sulfate ( $\text{HSO}_4^-$   
254  $/\text{SO}_4^{2-}$ ) and  $\text{S}_3^{2-}$  ion, and provide redox and acidity (pH) buffering of the system (e.g., 29, 33). In situ X-  
255 ray absorption spectroscopy (XAS) measurements at Pt  $L_3$ -edge (11.564 keV) were performed at BM30-  
256 FAME beamline of the European Synchrotron Radiation Facility (ESRF, Grenoble, France), using a  
257 hydrothermal apparatus developed at the Néel Institute. This setup enables simultaneous acquisition of  
258 high-quality fluorescence spectra from dilute solutions (down to 0.1 mmol Pt) to extract ligand identity,  
259 molecular structure and metal redox state and to directly determine the total dissolved Pt concentration  
260 (33). Measurements were conducted at 275°C and 700 bar. The XAS experiments were complemented  
261 by batch-reactor measurements of PtS(s) solubility at similar conditions (300°C, 500 bar) using  
262 hydrothermal reactors allowing controlled sampling or quenching of the fluid that was processed and  
263 analyzed using recent protocols developed for trace metals in S-rich solutions (20).

264 **Molecular simulations and XANES spectra modeling.** Both static Density Functional Theory (DFT)  
265 and First Principles Molecular Dynamics (FPMD) simulations of the geometries and interatomic  
266 distances of selected [Pt-HS- $\text{S}_3$ ]-type complexes were performed following approaches developed for a  
267 similar Au- $\text{HS}^-/\text{H}_2\text{S}-\text{S}_3^{2-}$  system (29). The calculated molecular structures were compared with  
268 experimental XAS-derived distances and coordination numbers to better constrain the stoichiometry of  
269 complexes. In addition, XANES spectra of such complexes were simulated using the FDMNES package  
270 (*SI Appendix*) and compared with the experimental spectra to further constrain the Pt coordination and  
271 oxidation state in the fluid phase.

272 **Thermodynamic analysis of platinum speciation and solubility.** Platinum solubility in experimental  
273 solutions was modeled in terms of dominant [Pt-HS- $\text{S}_3$ ] complexes using the constraints imposed by the  
274 spectroscopic and molecular data, and based on available robust thermodynamic properties of aqueous  
275 sulfur species including  $\text{S}_3^{2-}$  (*SI Appendix*, Table S3). The derived stoichiometries and formation  
276 constants for the two dominant  $\text{Pt}^{\text{II}}$  and  $\text{Pt}^{\text{IV}}$  complexes (reactions [1] and [2]) are consistent with the  
277 whole set of experimental data. The generated reaction constants values allow PtS(s) solubility to be  
278 predicted in S-bearing epithermal fluids (~300°C, 500 bar) as a function of pH, oxygen fugacity and total  
279 sulfur content with an overall precision of better than  $\pm 1$  order of magnitude (*SI Appendix*).

280

## 281 **Acknowledgements**

282 This work was funded by the French National Research Agency (grant RadicalS, ANR-16-CE31-0017), the Institut  
283 Carnot ISIFoR (grant OrPet), and the Centre National de la Recherche Scientifique (grant PtS3, MétalloMix-2021).  
284 We acknowledge the European Synchrotron Radiation Facility (ESRF) for access to beam time and infrastructure,  
285 and the Grand Equipement National for Calcul Intensif (GENCI) and the Institut du Développement et des

286 Ressources en Informatique Scientifique (IDRIS) for access to computing facilities. The FAME-UHD project is  
 287 supported by the French Grand Emprunt EquipEx (EcoX ANR-10-EQPX-27-01), the CEA-CNRS CRG consortium  
 288 and the INSU-CNRS. The Cluster of Excellence MATISSE led by Sorbonne University is supported by the ANR  
 289 Investissement d’Avenir (ANR-11-IDEX-0004-02). A. Colin, I. Kieffer, E. Lahera, O. Proux, and A. Seitsonen are  
 290 acknowledged for help with the synchrotron experiments and FPMD calculations. Special thanks go to A-M. Cousin  
 291 for assistance with figure layout and to Y. Joly for advice on XANES modeling. Comments of the Editor and two  
 292 anonymous referees greatly improved this article.

293

## 294 References

- 295 1. V. W. W. Yam, Behind platinum’s sparkle. *Nat. Chem.* **2**, 790 (2010).
- 296 2. G. Gunn, *Critical Metals Handbook*. Wiley (2014).
- 297 3. J. M. Brennan, The platinum-group elements: “admirably adapted” for science and industry. *Elements* **4**,  
 298 227–232.
- 299 4. J. E. Mungall (ed.), Exploration for platinum-group elements deposits. *Min. Assoc. Canada Short Course*  
 300 **35**, 1–494 (2005).
- 301 5. S-J. Barnes, E. M. Ripley, Highly siderophile and strongly chalcophile elements in magmatic deposits.  
 302 *Rev. Mineral. Geochem.* **81**, 725–774 (2016).
- 303 6. C. G. Ballhaus, E.F. Stumpfl, Sulfide and platinum mineralization in the Merensky Reef: evidence from  
 304 hydrous silicates and fluid inclusions. *Contrib. Mineral. Petrol.* **94**, 193–204 (1986).
- 305 7. S. Arai, M. Miura, Formation and modification of chromitites in the mantle. *Lithos* **264**, 277–295 (2016).
- 306 8. A. Boudreau, *Hydromagmatic Processes and Platinum-group Elements in Layered Intrusions*. Cambridge  
 307 Univ. Press, 1–275 (2019).
- 308 9. M. Rehkämper, A. N. Halliday, D. Barfod, J. G. Fitton, J. B. Dawson, Platinum-group element abundance  
 309 patterns in different mantle environments. *Science* **278**, 1595–1598 (1997).
- 310 10. A. Luguët, D. G. Pearson, G. M. Nowell, S. T. Dreher, J. A. Coggon, Z. V. Spetsius, S. W. Parman,  
 311 Enriched Pt-Re-Os isotope systematics in plume lavas explained by metasomatic sulfides. *Science*  
 312 **319**, 453–456 (2008).
- 313 11. S. A. Wood, The aqueous geochemistry of the platinum-group elements with applications to ore deposits.  
 314 In: *The Geology, Geochemistry, Mineralogy and Mineral Beneficiation of Platinum-Group Elements*,  
 315 ed. L.J. Cabri, *Canadian Institute of Mining, Metallurgy and Petroleum Special Volume* **54**, 211–250  
 316 (2002).
- 317 12. T. S. Ahmadi, Z. L. Wang, T. C. Green, A. Hendlein, M. A. El-Sayed, Shape-controlled synthesis of  
 318 colloidal platinum nanoparticles. *Science* **272**, 1924–1926 (1996).
- 319 13. L. Chong et al., Ultralow-loading platinum-cobalt fuel cell catalysts derived from imidazolate  
 320 frameworks. *Science* **362**, 1276–1281 (2018).
- 321 14. I. Lee, R. Morales, M. A. Albiter, F. Zaera, Synthesis of heterogeneous catalysts with well shaped  
 322 platinum particles to control reaction selectivity. *Proc. Natl. Acad. Sci. U.S.A.* **105**, 15241–15246  
 323 (2008).
- 324 15. D. C. Sassani, E. L. Shock, Solubility and transport of platinum-group elements in supercritical fluids:  
 325 Summary and estimates of thermodynamic properties for ruthenium, rhodium, palladium, and  
 326 platinum solids, aqueous ions, and complexes to 1000°C and 5 kbar. *Geochim. Cosmochim. Acta* **62**,  
 327 2643–2671 (1998).
- 328 16. E. F. Bazarkina, G. S. Pokrovski, J.-L. Hazemann, Structure, stability and geochemical role of palladium  
 329 chloride complexes in hydrothermal fluids. *Geochim. Cosmochim. Acta* **146**, 107–131 (2014).

- 330 17. B. R. Tagirov, O. N. Filimonova, A. L. Trigub, N. A. Akinfiev, M. S. Nickolsky, K. O. Kvashnina, D. A.  
331 Chareev, A. V. Zotov, Platinum transport in chloride-bearing fluids and melts: insights from in-situ X-  
332 ray absorption spectroscopy and thermodynamic modeling. *Geochim. Cosmochim. Acta* **254**, 86–101  
333 (2019).
- 334 18. F. A. Cotton, G. Wilkinson, C. A. Murillo, M. Bochmann, *Advanced Inorganic Chemistry*, 6<sup>th</sup> Edition,  
335 Wiley, Chichester (1999).
- 336 19. C. H. Gammons, M. S. Bloom, Experimental investigation of the hydrothermal geochemistry of platinum  
337 and palladium: II. The solubility of PtS and PdS in aqueous sulfide solutions to 300°C. *Geochim.*  
338 *Cosmochim. Acta* **57**, 2451–2467 (1993).
- 339 20. M. A. Kokh, N. N. Akinfiev, G. S. Pokrovski, S. Salvi, D. Guillaume, The role of carbon dioxide in the  
340 transport and fractionation of metals by geological fluids. *Geochim. Cosmochim. Acta* **197**, 433–466  
341 (2017).
- 342 21. O. N. Filimonova, B. R. Tagirov, A. V. Zotov, N. N. Baranova, Y. V. Bychkova, D. A. Tyurin, D. A.  
343 Chareev, M. S. Nickolsky, The solubility of cooperate PtS(cr) at 25–450°C,  $P_{\text{sat}}$ –1000 bar and  
344 hydrosulfide complexing of platinum in hydrothermal fluids. *Chem. Geol.* **559**, 119968 (2021).
- 345 22. P. Pan, S. A. Wood, Solubility of Pt and Pd sulfides and Au metal in aqueous bisulfide solutions. II.  
346 Results at 200° to 350°C and saturated vapor pressure. *Min. Deposita* **29**, 373–390 (1994).
- 347 23. T. Chivers, P. J. W. Elder, Ubiquitous trisulfur radical ion: fundamentals and applications in materials  
348 science, electrochemistry, analytical chemistry and geochemistry. *Chem. Soc. Rev.* **42**, 5996–6005  
349 (2013).
- 350 24. G. S. Pokrovski, L. S. Dubrovinsky, The  $S_3^-$  ion is stable in geological fluids at elevated temperatures  
351 and pressures. *Science* **331**, 1052–1054 (2011).
- 352 25. N. Jacquemet, D. Guillaume, A. Zwick, G. S. Pokrovski, In situ Raman spectroscopy identification of the  
353  $S_3^-$  ion in S-rich hydrothermal fluids from synthetic fluid inclusions. *Amer. Miner.* **99**, 1109–1118  
354 (2014).
- 355 26. G. S. Pokrovski, J. Dubessy, Stability and abundance of the trisulfur radical ion  $S_3^-$  in hydrothermal  
356 fluids, *Earth Planet. Sci. Lett.* **411**, 298–309 (2015).
- 357 27. G. Barré, L. Truche, E. F. Bazarkina, R. Michels, J. Dubessy, First evidence of the trisulfur radical ion  
358  $S_3^-$  and other sulfur polymers in natural fluid inclusions. *Chem. Geol.* **462**, 1–14 (2017).
- 359 28. A. Colin, C. Schmidt, G. S. Pokrovski, M. Wilke, A. Y. Borisova, M. J. Toplis, *In situ* determination of  
360 sulfur speciation and partitioning in aqueous fluid-silicate melt systems. *Geochem. Persp. Lett.* **14**, 31–  
361 35 (2020).
- 362 29. G. S. Pokrovski, M. A. Kokh, D. Guillaume, A. Y. Borisova, P. Gisquet, J.-L. Hazemann, E. Lahera, W.  
363 Del Net, O. Proux, D. Testemale, V. Haigis, R. Jonchière, A.P. Seitsonen, G. Ferlat, R. Vuilleumier,  
364 A. M. Saitta, M.-C. Boiron, J. Dubessy, Sulfur radical species form gold deposits on Earth. *Proc. Natl.*  
365 *Acad. Sci. U.S.A.* **112**, 13484–13489 (2015).
- 366 30. ICSD - *Inorganic Crystal Structure Database*, FIZ Karlsruhe, 2021, [https://icsd.products.fiz-](https://icsd.products.fiz-karlsruhe.de/)  
367 [karlsruhe.de/](https://icsd.products.fiz-karlsruhe.de/) [accessed 18 May 2021].
- 368 31. T. Imaoka, Y. Akanuma, N. Haruta, S. Tsuchiya, K. Ishihara, T. Okayasu, W.-J. Chun, M. Takashashi, K.  
369 Yamamoto, Platinum clusters with precise numbers of atoms from preparative-scale catalysis. *Nat.*  
370 *Comm.* **8**, 688 (2017).
- 371 32. H. Häkkinen, The gold-sulfur interface at the nanoscale. *Nat. Chem.* **4**, 443–455 (2012).
- 372 33. G. S. Pokrovski, B. R. Tagirov, J. Schott, J.-L., Hazemann, O. Proux, A new view on gold speciation in  
373 sulfur-bearing hydrothermal fluids from in-situ X-ray absorption spectroscopy and quantum-chemical  
374 modeling, *Geochim. Cosmochim. Acta* **73**, 5406–5427 (2009).

375

376 **Figure captions**

377

378

379 **Fig. 1.** Platinum L<sub>3</sub>-edge XANES spectra of S-bearing aqueous solutions in equilibrium with PtS(s) at  
 380 indicated pH and oxygen fugacity (relative to the conventional hematite-magnetite mineral buffer, HM)  
 381 recorded at 275°C and 700 bar and compared with reference compounds (A) and quantum-chemistry  
 382 simulated XANES spectra of representative [Pt-HS-S<sub>3</sub>]-type complexes with structures optimized using  
 383 molecular modeling (B). Vertical dashed lines are an eye guide to indicate differences in the experimental  
 384 spectra (A) with changes of pH and oxygen fugacity, and (B) among the calculated spectra of the shown Pt<sup>II</sup>  
 385 and Pt<sup>IV</sup> species (see *SI Appendix, Fig. S1A* and Table S1 for solution composition and speciation).

386

387

388 **Fig. 2.** Direct evidence for platinum-trisulfur ion complexes from PtS(s) solubility measurements in aqueous  
 389 thiosulfate solutions as a function of pH and S<sub>3</sub><sup>2-</sup> ion concentration at 300°C and 500 bar. Thiosulfate  
 390 irreversibly breaks down on heating by providing sulfate, sulfide and S<sub>3</sub><sup>2-</sup> ion (*SI Appendix*). Symbols  
 391 represent the measured Pt concentrations (error bars = 2 SD); solid red line shows the predicted total Pt  
 392 solubility according to the speciation model of this study that includes the two indicated Pt<sup>II</sup> and Pt<sup>IV</sup>  
 393 complexes with S<sub>3</sub><sup>2-</sup> and HS<sup>-</sup> ligands (dotted blue and purple lines); dashed green curve shows the sum of  
 394 concentrations of Pt(HS)<sub>n</sub><sup>2-n</sup> complexes from the literature, where n = 2, 3 or 4 (19, 21); dashed black curves  
 395 indicate the free concentration of the two ligands, HS<sup>-</sup> and S<sub>3</sub><sup>2-</sup>. The break in the species curve pattern at pH  
 396 ~5 reflects the onset of molten sulfur (S<sub>liq</sub>) formation at more acidic pH (Table S3 for data sources and Fig.  
 397 S1B for details on S aqueous speciation).

398

399

400 **Fig. 3.** Platinum dissolved concentration in equilibrium with PtS(s) in hydrothermal fluid at 300°C and  
 401 500 bar and its comparison with gold as a function of (A) total dissolved S concentration at pH ~5 and f<sub>O2</sub>  
 402 buffered by sulfide-sulfate equilibrium with (H<sub>2</sub>S)<sub>tot</sub>:(SO<sub>4</sub>)<sub>tot</sub> molal ratio of 4:1 corresponding to the  
 403 maximum of S<sub>3</sub><sup>2-</sup> abundance; (B) oxygen fugacity corresponding to common redox buffers, QFM –  
 404 quartz-fayalite-magnetite, NNO – nickel-nickel oxide, PPM – pyrite-pyrrhotite-magnetite, and HM –  
 405 hematite-magnetite; (C) fluid acidity, pH = -log<sub>10</sub> a(H<sup>+</sup>) at f<sub>O2</sub> buffered by sulfide-sulfate equilibrium  
 406 (H<sub>2</sub>S:SO<sub>4</sub> = 4:1); (D) in equilibrium with gold metal as a function of pH at the conditions identical to (C).  
 407 In all panels, the curves denote the concentrations of S<sub>3</sub><sup>2-</sup> (blue, in µg/g of S, same scale as for Pt and Au),  
 408 sum of known Pt/Au-Cl, Pt/Au-HS, Pt-SO<sub>4</sub> and Au-OH species (green) and the total Pt or Au solubility  
 409 (red) including Pt(HS)<sub>2</sub>(S<sub>3</sub>)<sub>2</sub><sup>2-</sup> and Pt(HS)<sub>3</sub>(H<sub>2</sub>O)(S<sub>3</sub>)<sub>2</sub><sup>-</sup> or Au(HS)S<sub>3</sub><sup>-</sup>. The difference between the two  
 410 latter curves (vertical pink arrow), corresponds to the contribution of [Pt-S<sub>3</sub><sup>-</sup>]- or [Au-S<sub>3</sub><sup>-</sup>]-type  
 411 complexes. The thermodynamic properties of Au/Pt-Cl-HS-SO<sub>4</sub> species and other fluid constituents are  
 412 from Table S3.

413

